Wang *et al. Biochar* (2025) 7:100
https://doi.org/10.1007/s42773-025-00493-9

Biochar

ORIGINAL RESEARCH Open Access

The dose-dependent effects of dissolved biochar on *C. elegans*: insights into the physiological and transcriptomic responses

Xinrui Wang[1], Jie Li[1*], Lan Luo[1], Gang Li[1], Yan Xu[1], Weibin Ruan[2] and Guilong Zhang[1*]

Abstract

As the benefits of biochar amendment for soil remediation have been widely recognized, the potential risk of downward nematode migration has received increasing attention. Dissolved biochar (DBC) is an essential component of biochar that is easily absorbed and utilized by organisms. However, the effect of DBC on nematodes remains unclear. This study aimed to assess the effect of DBC on *Caenorhabditis elegans*. The response of *C. elegans* to different DBC concentrations (0, 250, 500, and 1000 mg L^{-1}) was investigated using culture assays and RNA-seq analysis. The results revealed a hormetic effect of DBC, with low concentrations (250–500 mg L^{-1}) promoting growth and high concentrations (≥ 1000 mg L^{-1}) inhibiting growth. Meanwhile, DBC affected nematode movement and neuromuscular function. Transcriptome analysis revealed a dose-dependent increase in the number of differentially expressed genes (DEGs), with key changes related to metabolism, the stress response, and cellular processes. Weighted gene coexpression network analysis (WGCNA) revealed that gene modules, such as *dyf-11*, *ins-16*, and *hsp-12.6*, were strongly correlated with traits such as body size and reproduction. Additionally, genes involved in ciliary function, insulin signaling, and neurotransmitter biosynthesis were affected, highlighting the impact of DBC on growth and movement regulation. These findings suggest the need to carefully manage biochar application in agriculture to balance its benefits and potential risks to soil organisms like nematodes.

Highlights

- Worms can ingest dissolved biochar (DBC).
- Low-dose DBC promoted worm growth, while high-dose DBC inhibited it.
- DBC exposure altered worm genes linked to growth, stress, and movement.

Keywords Dissolved biochar (DBC), *C. elegans*, Hormetic effect, Transcriptome analysis

*Correspondence:
Jie Li
lijie@caas.cn
Guilong Zhang
zhangguilong@caas.cn
Full list of author information is available at the end of the article

Graphical Abstract

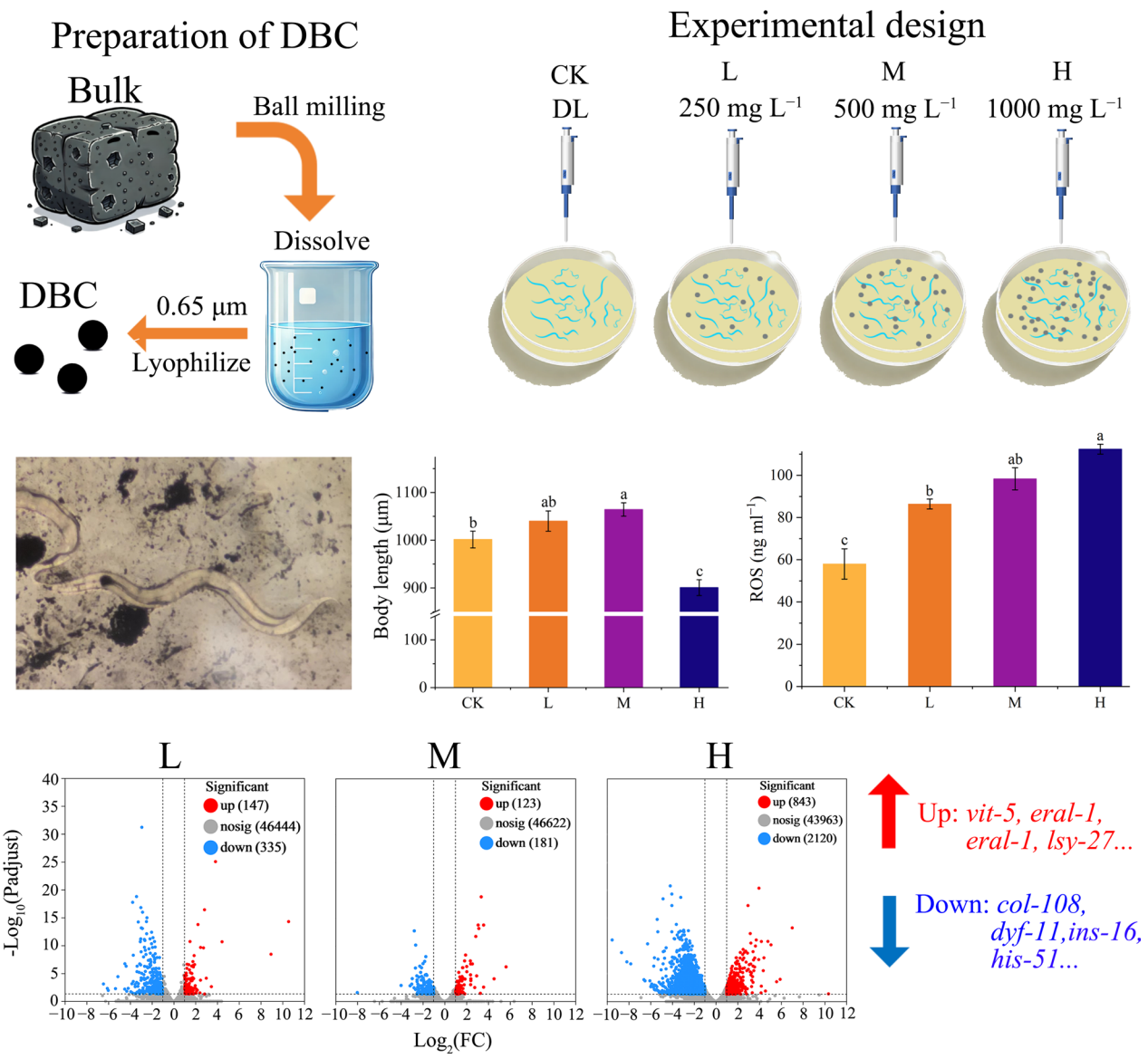

1 Introduction

Biochar is a pyrogenic carbonaceous material prepared under oxygen-limited conditions at temperatures ranging from 300 to 700 °C (Lehmann 2007), characterized by high carbon content, porosity, and adsorptive properties, which could contribute to its benefits in soil amendment and carbon sequestration (Lehmann et al. 2011; Wang et al. 2020; Nepal et al. 2023). Although biochar application had promising advantages for soil management, its inevitable dissolution and oxidation upon environmental exposure posed potential risks to the soil biota (Lian et al. 2019; Li et al. 2024b; Dong et al. 2025).

Nematodes occupy various trophic levels in soil and play crucial roles in the food web, soil quality, and nutrient cycling for maintaining soil health. In recent decades, significant attention has been paid to the environmental and health impacts of biochar application (Zhang et al. 2023; Long et al. 2024). Field studies reported that biochar improved the nutrient supply, which in turn increased the abundance of soil microorganisms. This increased microbial abundance

often led to greater populations of microbivorous and omnivorous nematodes, which relied on microbial communities as food sources (Jeffery et al. 2022; Liu et al. 2022a, 2024a). However, in certain cases, biochar amendment had toxic effects on nematodes. Li and Chen (2020) reported that biochar amendment resulted in reduced body length and lifespan of nematodes in culture-based assays. Additionally, studies by Lieke et al. (2018) and Alharbi et al. (2023) demonstrated that persistent free radicals or polycyclic aromatic hydrocarbons (PAHs) in biochar could inhibit nematode growth and induce avoidance behavior, indicating that the direct impact of biochar on nematodes is not always beneficial.

While most existing studies focused on bulk biochar, there remained a significant knowledge gap regarding the potential risks associated with its water-soluble fraction, known as dissolved biochar (DBC). DBC primarily consists of colloidal particles and a smaller proportion of nanobiochar particles, which result from the decomposition of biochar (Lian and Xing 2024). Due to their small size, DBC particles could migrate more easily through soil pores. Guggenberger et al. (2008) hypothesized that smaller biochar particles would exhibit stronger interactions with soil nematodes, potentially causing their migration into deeper soil layers. Therefore, compared with bulk biochar, DBC is characterized by greater environmental mobility and bioavailability (Lian and Xing 2017; Rombolà et al. 2023; Liu et al. 2024b). Prodana et al. (2019) reported that small particles of pine woodchip biochar posed sublethal toxicity risks to soil organisms, suggesting that the concentration of microbiochar was a key factor in disrupting soil biota. Furthermore, recent studies have demonstrated that the effects of DBC on soil organisms were complex. Qin et al. (2021) and Singh et al. (2022) noted that DBC had dual effects: it could serve as an exogenous labile carbon source for microorganisms, thereby enhancing microbial activity and indirectly benefiting nematode populations that depended on these microorganisms for food. However, high concentrations of DBC might exert toxic effects through mechanisms such as electron transfer, which were detrimental to nematodes (Yang et al. 2021; Da Costa et al. 2024). Nevertheless, the threshold and molecular mechanisms through which DBC affects nematodes remained inadequately understood.

This study investigated the role of dissolved biochar in nematode biology, hypothesizing that the DBC could exert distinct and dual effects on nematodes. We proposed that DBC particles interact with nematodes in a dose-dependent manner, thereby influencing their feeding behavior, development, and gene expression. Furthermore, through transcriptomic analysis, this research aimed to identify gene expression changes induced by DBC exposure, thus mapping molecular pathways related to growth, reproduction, and stress responses. The objectives of this study are: (1) to characterize DBC, including its particle size, elemental composition, and functional groups; (2) to assess the effects of different DBC concentrations on the feeding behavior and development of *C. elegans*; and (3) to conduct transcriptome sequencing analysis of *C. elegans* exposed to different DBC concentrations. This study may provide essential insights for the interactions between biochar and soil fauna, as well as for evaluating the safety implications of nano/micro biochar application, thus informing both ecological and toxicological assessments.

2 Materials and methods

2.1 Preparation and characterization of dissolved biochar

Corn straw was used as the raw material to prepare biochar in a muffle furnace (HBYQ 2200). After smashing, the feedstock was slowly pyrolyzed (10 °C min^{-1}) at 700 °C under N_2 for 2 h. The obtained biochar was ground, sieved through a 0.15-mm mesh and labeled as bulk biochar (BC700).

DBC (DBC700) was prepared in a combined procedure involving ball milling, sedimentation and filtration. First, the obtained biochar was ground to powder by a planetary ball mill with a ball:powder ratio of 20:1 and a constant rotation speed of 350 RPM for 12 h. Second, 50 g of the ball-milled biochar was mixed with 1 L of deionized (DI) water and stirred (150 RPM) at room temperature for 24 h (1:20 solid:liquid ratio). After sonication (2 h at 100 W), the suspension was slowly filtered through a 0.65-μm filter, and the DBC in the filtrate was measured. A portion of the filtrate was stored at 4 °C, and the total dissolved organic matter (DOM) content was measured within 48 h. The remainder was freeze-dried at −70 °C. The concentration of DBC was defined by the amount of freeze-dried biochar used in the preparation of a 1000 mg biochar L^{-1} solution, and after serial dilution with DI water, the required concentrations (250 and 500 mg L^{-1}) were obtained.

The DOM concentration was determined using a total organic carbon analyzer (TOC-L CPN, Shimadzu, Japan). The elemental composition (C, H, N, and O) of the freeze-dried biochar was determined by elemental analysis (EA3000, Leeman, Italy). The specific surface area (SSA) was measured using the Brunauer–Emmett–Teller (BET) method with an automatic gas adsorption analyzer (3Flex, Micromeritics, USA) at a temperature of −195 °C, with nitrogen adsorption and desorption cycles performed at 15-s intervals. Three-dimensional fluorescence (EEM) spectra were measured using a fluorescence spectrophotometer (F-700, Hitachi, Japan).

The functional groups were characterized by Fourier transform infrared (FTIR) spectroscopy with a resolution in the wavenumber range from 400 to 4000 cm^{-1}. The particle size was determined using a particle size analyzer (Mastersizer 3000, Malvern, England). The environmentally persistent free radicals (EPFRs) were detected using a Bruker EMXplus electron paramagnetic resonance spectrometer (Germany). Singlet oxygen, superoxide radicals, and hydroxyl radicals ($^1O_2$, O_2^-, –OH) of DBC were measured by an Electron Spin Resonance (ESR) spectrometer, Magnettech (ESR 5000, Bruker, Germany), and the total spin count and molar spin concentration were calculated through second integration for semi-quantitative analysis.

2.2 Nematode culture

This study used *Caenorhabditis elegans* because of its transparent body and available complete genome sequence. Wild-type N2 (Bristol) *C. elegans* worms were obtained from SunyBiotech Company, and the worms were maintained on nematode growth medium (NGM) with *E. coli* OP50 at 22 °C. In an NGM plate without OP50, 30 fully fed adult hermaphrodites were transferred via a platinum wire pick and allowed to lay eggs for 7–9 h. To achieve synchronized hatching, OP50 was not added at the moment, so that the first-laid eggs could hatch in the absence of food. After adequate L1-stage larvae were present on each NGM plate, the adults were removed. Then, food was added to allow the larvae to grow to the L2 stage for subsequent DBC exposure experiments.

2.3 Measurement of the phenotype, stress response and reproduction of *C. elegans*

The prepared L2-stage worms were exposed to 0.5 mL of DBC solution at different concentrations (250, 500, and 1000 mg L^{-1}) in NGM with OP50, with an equal volume of sterile deionized water used as the control (CK). The phenotype and stress response of *C. elegans* individuals were measured under an Olympus SZX16 microscope with cellSens Dimension software when they reached the adult stage.

The body size of *C. elegans*, including body length and width, was measured when they reached the adult stage as described by Woodruff et al. (2018) to assess individual worm development. Moreover, the body bending frequency of the nematodes was measured within 60 s to test the stress response, as described by Nawa and Matsuoka (2012).

Additionally, reproduction assays were carried out after morphological observation. One L4-stage worm was transferred to each Petri dish (3.5 cm) containing 50 µL of OP50 in LB medium, with a total of 17 worms for each treatment and the control. Nematodes were grown at 25 °C for 72 h, and the number of worms at all stages except the egg stage was recorded to evaluate the reproduction of worms exposed to DBC.

2.4 SOD, CAT, ROS test of *C. elegans*

The concentrations of superoxide dismutase (SOD), catalase (CAT), and reactive oxygen species (ROS) in the treatments (CK, L, M, H) were quantified using commercial ELISA kits, following the manufacturer's protocol.

Briefly, a total of 50 µL of standard solution was added to the designated standard wells. That is, 10 µL of sample (CK, L, M, H) and 40 µL of sample diluent were added to the corresponding wells. The blank wells received no reagents. Subsequently, 100 µL of HRP–conjugate reagent was added to each well. The plate was covered with an adhesive film and incubated at 37 °C for 60 min. After incubation, wells were aspirated and washed five times with 400 µL of wash solution per well. Any residual liquid was carefully removed by blotting the plate on absorbent paper. Next, 50 µL each of Chromogen Solutions A and B were added to all wells. The plate was gently mixed and incubated at 37 °C for 15 min in the dark. Then, 50 µL of Stop Solution was added to each well, changing the color from blue to yellow. Absorbance at 450 nm was measured within 15 min using a microplate reader. Final concentrations of SOD, CAT, and ROS were calculated by comparing the optical density (O.D.) of test samples with the standard curve derived from serially diluted standards.

2.5 Transcriptome sequencing

Once the *C. elegans* individuals in each treatment group grew into young adult worms, they were collected, treated with liquid nitrogen, and then stored at − 80 °C for RNA sequencing (RNA-seq) and transcriptomic analysis.

Total RNA was extracted from tissue using TRIzol® Reagent according to the manufacturer's instructions. The RNA quality was subsequently determined with a 5300 Bioanalyzer (Agilent) and quantified using an ND-2000 (NanoDrop Technologies). Only high-quality RNA samples (OD260/280 = 1.8–2.2, OD260/230 ≥ 2.0, RQN ≥ 6.5, 28S:18S ≥ 1.0 > 1 µg) were used to construct a sequencing library.

RNA purification, reverse transcription, library construction and sequencing were performed at Shanghai Majorbio Bio-pharm Biotechnology Co., Ltd. (Shanghai, China) according to the manufacturer's instructions for the kits and instruments used. The RNA-seq transcriptomic library was prepared following the Illumina® Stranded mRNA Prep, Ligation (San Diego, CA) protocol, using 1 µg of total RNA. Briefly, messenger

RNA was first isolated by the poly(A) selection method with oligo(dT) beads and then fragmented with fragmentation buffer. Second, double-stranded cDNA was synthesized using a SuperScript Double-Stranded cDNA Synthesis Kit (Invitrogen, CA) with random hexamer primers. The synthesized cDNA was subsequently subjected to end repair, phosphorylation and adapter addition according to the library construction protocol. Libraries were size-selected for 300 bp cDNA target fragments on 2% Low Range Ultra Agarose, followed by amplification using Phusion DNA polymerase (NEB) for 15 PCR cycles. After quantification with a Qubit 4.0, library sequencing was performed on a NovaSeq X Plus platform (PE150) using a NovaSeq Reagent Kit or on the DNBSEQ-T7 platform (PE150) using a DNBSEQ-T7RS Reagent Kit (FCL PE150), version 3.0. The raw paired-end reads were trimmed and quality controlled using *fastp* with default parameters. Then, the clean reads were separately aligned to the reference genome in orientation mode using HISAT2 (Kim et al. 2015) software. The mapped reads of each sample were assembled by StringTie (Pertea et al. 2015) in a reference-based approach.

2.6 Quantitative RT–PCR

The mRNA samples were extracted, and a PCR master mix was prepared using ChamQ SYBR Color qPCR Master Mix 2X, along with forward primer (Primer F), reverse primer (Primer R), template DNA, and ddH_2O. The reaction was conducted using a LineGene 9600 Plus fluorescence quantitative PCR instrument (Bioer, China). For each gene analyzed, expression levels were normalized to the reference gene, *pmp-3*, across three independent biological replicates (Zhang et al. 2011). In accordance with the physiological variation in *C. elegans* observed in this study, the selected differentially expressed genes (*perm-4*, *abf-2*, *col-108*, *his-51*, and *msp-3*) were validated by real-time quantitative reverse transcription PCR (qRT–PCR). Finally, the relative expression ratios of the target genes were calculated using the ΔΔCt method to maintain rigorous scientific standards.

2.7 Statistical analysis

Data on the body development and reproduction of *C. elegans* were recorded using Microsoft Excel. The statistical significance of the observed alterations was assessed using R software (ggplot2, DescTools) for data visualization and one-way ANOVA (Duncan's test). A p-value of < 0.05 was considered statistically significant.

To identify differentially expressed genes (DEGs) between two different samples, the expression level of each transcript was calculated according to the transcripts per million reads (TPM) method. RSEM (Li and Dewey, 2011) was used to quantify gene abundances. Differential expression analysis was performed using DESeq2 (Love, et al., 2014). DEGs with $|\log_2 FC| \geq 1$ and FDR < 0.05 (DESeq2) were considered significantly differentially expressed genes.

In addition, functional enrichment analyses, including GO and KEGG analyses, were performed to identify which DEGs were significantly enriched in GO terms and metabolic pathways at a Bonferroni-corrected P value < 0.05 compared with the whole-transcriptome background. GO functional enrichment and KEGG pathway analyses were carried out using the Gene Ontology database (http://www.geneontology.org/), R (ClusterProfiler) Python scipy and KAAS (https://www.genome.jp/tools/kaas/). WGCNA was performed using Mfuzz time series software.

3 Results and discussion

3.1 Characterization of the dissolved biochar

To determine the impact of dissolved biochar (DBC) on soil nematodes and investigate its underlying mechanisms, the physical and chemical properties of DBC were analyzed to understand its potential risks and benefits. Scanning electron microscopy (SEM) images revealed that the morphology of the biochar particles was predominantly spherical or irregular, with a wide range of particle sizes and levels of surface roughness (Fig. 1a). These morphological characteristics were attributed to the specific preparation processes used for DBC (Ng et al. 2022). In this study, ball milling not only reduced the particle size but also likely induced reconstruction of the carbon surface, resulting in the formation of new surface morphologies and microstructures.

The particle size distribution of the DBC revealed the existence of a certain proportion of small particles. The D10, D50 and D90 values were 0.025 μm, 0.01 μm, and 4.15 μm, respectively (Table 1), suggesting that approximately half of the biochar particles were physically broken down into colloidal and nanosized fractions. Moreover, elemental analysis demonstrated that the carbon, oxygen, hydrogen, and nitrogen contents of DBC were 14.2%, 15.85%, 1.40 and 0.73%, respectively, which resulted in H/C and (O + N)/C ratios of 0.10 and 1.13, respectively. Similarly, Ma et al. (2019) reported an H/C ratio of 0.17 for micro- and nano- scale rice husk biochar. According to Zhang et al. (2011, 2017), the H/C and (O + N)/C ratios of biochar indicated its aromaticity and polarity. These results revealed that the atomic and polar indices of the DBC were closer to those of the colloidal and nanosized biochar than to bulk biochar. Moreover, the main components of DBC were humic

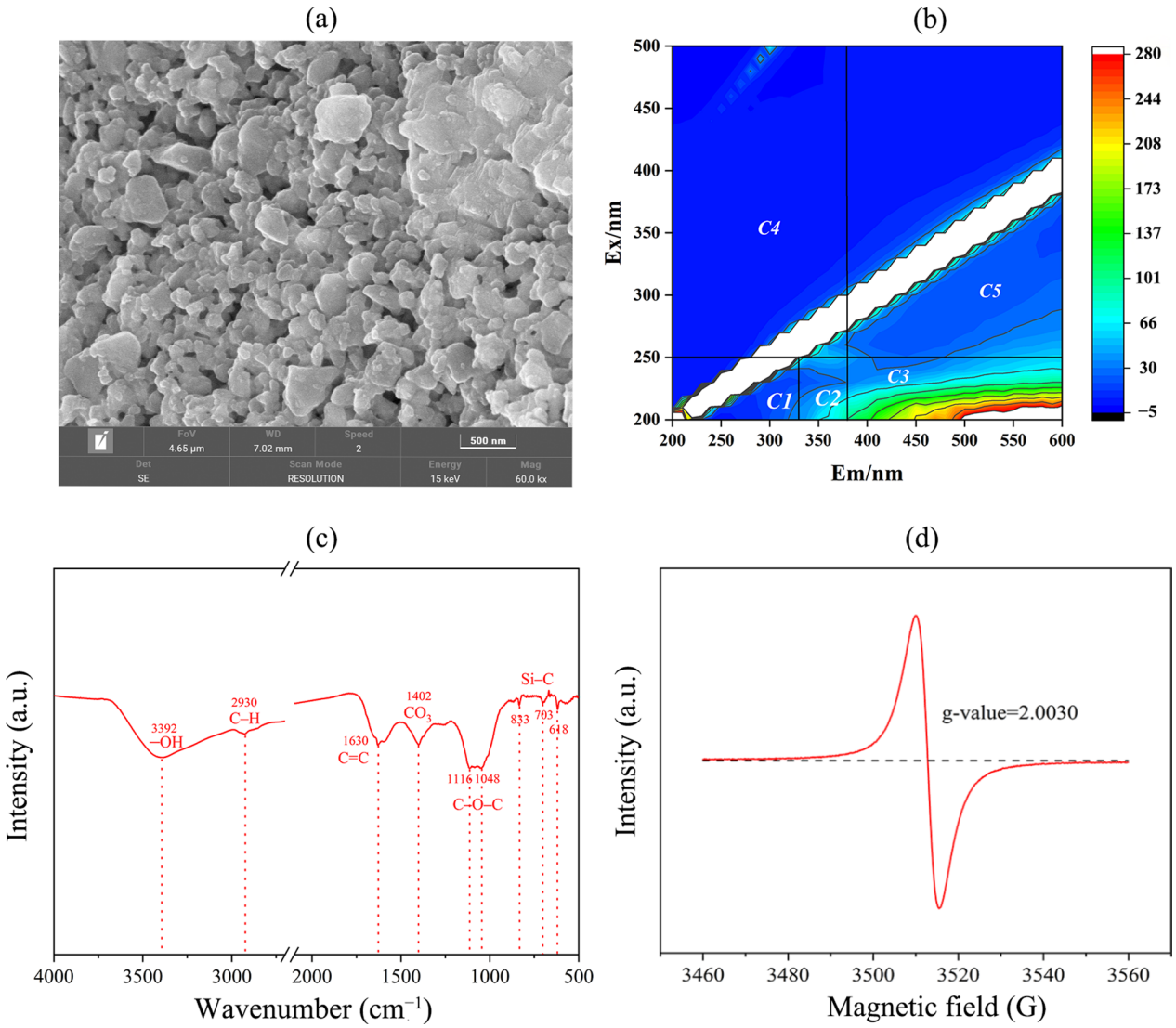

Fig. 1 SEM images (**a**), EEM images (**b**), FTIR spectra (**c**) and EPFRs (**d**) of the particles derived from the dissolved biochar

Table 1 Proximate analysis and particle size of the dissolved biochar

Sample	C (%)	H (%)	N (%)	O (%)	H/C	(O + N)/C	Average particle size (μm)		
							Dx10	Dx50	Dx90
DBC700	14.2	1.4	0.73	15.85	0.10	1.13	0.025	0.10	4.15

acid-like and fulvic acid-like components, accounting for 82.16% of the total components (Fig. 1b, Fig. S1). These humic and fulvic acid-like components could be served as carbon sources for microorganisms, including nematodes, among others (Tian et al. 2022).

The Fourier-transform infrared (FTIR) spectrum further confirmed the polar properties of the DBC samples, including –OH stretching (approximately 3400 cm^{-1}), C–O stretching (spanning from 1250 to 1000 cm^{-1}), and C–H bending vibrations (approximately 1400 cm^{-1}). The pronounced –OH and C–O stretching signals indicated a prevalence of aliphatic chains within the DBC (Fig. 1c).

Additionally, environmentally persistent free radicals (EPFRs) of the DBC were detected as evidenced by a g–value of 2.0030 (Fig. 1d), suggesting the presence of

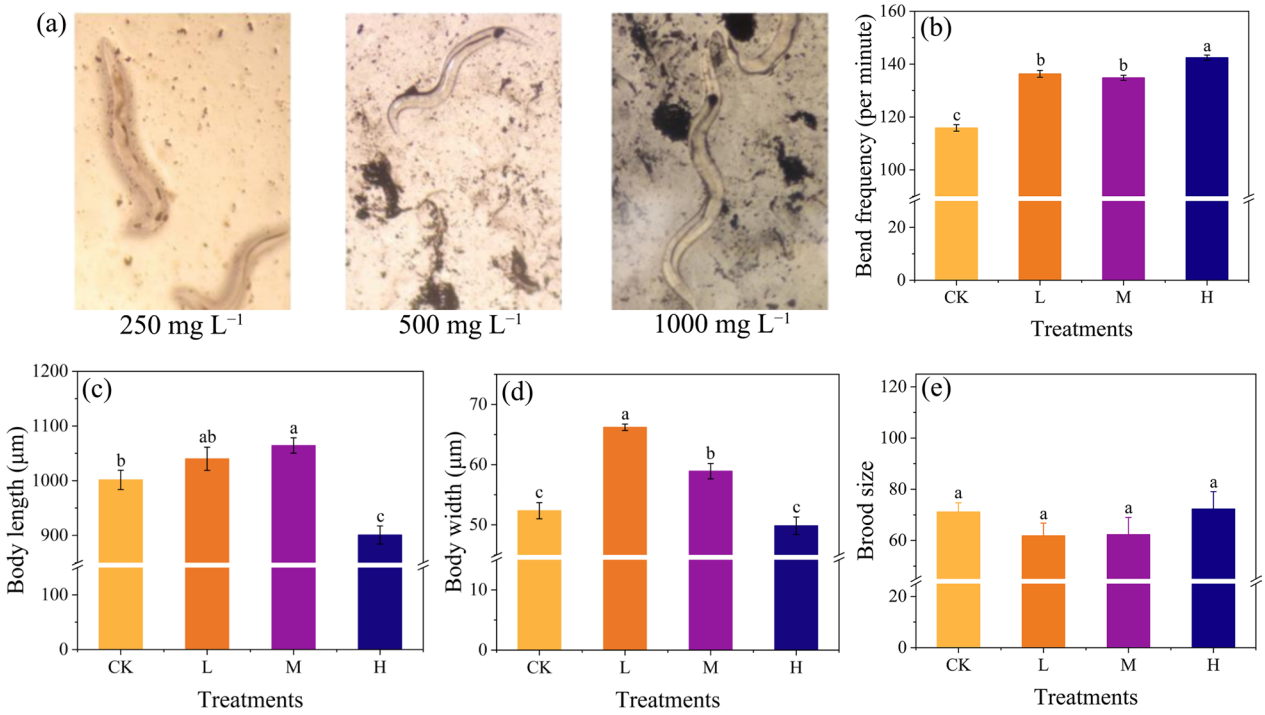

Fig. 2 Feeding behavior, body development and reproduction of *C. elegans* under different DBC concentrations (CK: 0 mg L^{-1}; low concentration (L): 250 mg L^{-1}; moderate concentration (M): 500 mg L^{-1}; high concentration (H): 1000 mg L^{-1}). **a** Feeding behavior. **b** Body bending. **c** Body length. **d** Body width. **e** Brood size

carbon-centered radicals with nearby oxygen atoms, aligning with findings by Jiang et al. (2024). EPFRs could induce the production of highly reactive oxygen species (ROS) in the environment, which might be associated with oxidative stress in biological organisms. The elevated ROS was correlated with the damage of membrane lipid proteins and even DNA (Liu et al. 2022b). Notably, the EPFR signal intensity of DBC in this study was significantly greater than that of the bulk biochar (Fig. S2), likely due to its greater degree of fragmentation and increased number of surface oxygen-containing functional groups. This finding also suggested that excessive exposure to DBC may cause oxidative damage in nematodes.

3.2 Effects of DBC on the feeding behavior, body development and reproduction of *C. elegans*

C. elegans were exposed to DBC at low (L, 250 mg L^{-1}), moderate (M, 500 mg L^{-1}) and high (H, 1000 mg L^{-1}) concentrations in comparison with the control group maintained in deionized water (CK). After exposure, the feeding behavior of *C. elegans* was observed beginning at the L2 stage. It was evident that *C. elegans* could move through and live around the biochar particles, displaying an obvious swallowing process (Fig. 2a). More details are also provided in the video in the Supporting Information. According to previous studies, the carbon content from biochar might help soil fauna mitigate food shortages (Lehmann et al. 2011; Hou et al. 2022). In our study, the D10, D50, and D90 values indicated a substantial abundance of colloidal and nanosized particles capable of being ingested by nematodes. The observed feeding behavior suggested that DBC did not pose immediate toxicity risks at the tested concentrations.

Given that nematodes survived while feeding with DBC, the effects of DBC on body bending, body development and reproduction in *C. elegans* were further investigated. As shown in Fig. 2b, a greater frequency of body bending in *C. elegans* in the DBC groups was detected. Compared with that in the CK (115 per minute), the average body bending frequencies in the 250, 500, and 1000 mg L^{-1} treatments increased to 136, 135, and 142 per minute, respectively. According to prevous studies, body bending behavior was a well-established indicator of neuromuscular activity in *C. elegans*, and it can be influenced by various environmental factors (Gu et al. 2024; Li et al. 2024b). Therefore, the increased body bending frequency of *C. elegans* exposed to DBC could indicate a stimulatory effect on the nematode's neuromuscular system. It was hypothesized that the EPFRs and functional groups of DBC might interact

with neurotransmitter pathways, influencing synaptic transmission and motor control (Li et al. 2024a).

Moreover, the consistent increase in bending frequency across all DBC-treated groups suggested that the interaction did not lead to overt toxicity (Li et al. 2024c; Perni et al. 2021) but rather stimulated normal motor activity. These findings are consistent with other studies showing that exposure to sublethal concentrations of nanoparticles or chemicals resulted in increased locomotor activity in *C. elegans* (Ellegaard-Jensen et al. 2012; Mani et al. 2024). However, our results were different from those of studies showing reduced locomotor activity or even paralysis upon exposure to higher concentrations of certain toxicants, such as heavy metals or polystyrene microplastics (Yu et al. 2020; Zhang et al. 2021). This differential response noted the unique interaction between DBC and the *C. elegans* neuromuscular system, implying that the effects of DBC are more closely associated with the modulation of neural activity than with neurotoxicity.

Unlike the effect on body bending behavior, exposure to DBC resulted in a hormetic effect on the body size of *C. elegans*; that is, DBC promoted worm growth at low concentrations and inhibited worm growth at high concentrations (Fig. 2c, d). Among the treatments, the average body length of *C. elegans* significantly increased to 1040.02 ± 21.26 μm and 1064.34 ± 14.04 μm in the 250 mg L^{-1} and 500 mg L^{-1} treatments, respectively, but decreased to 900.67 ± 16.61 μm in the 1000 mg L^{-1} treatment. The changes in *C. elegans* body width were similar to those observed in body length. Additionally, no significant difference in the brood size of *C. elegans* was observed among the DBC treatments (Fig. 2e).

This hormetic effect on the body size of *C. elegans* may be due to the interaction of DBC with the nematode's cellular and metabolic pathways. The increase in body size at lower DBC concentrations could be attributed to the bioactive properties of organic components of DBC, such as fulvic acid and humic acid, which were known to enhance nutrient availability or interact with cellular systems to trigger mild stress responses that promoted growth (Hemmatzadeh et al. 2024). This response is similar to that observed with carboxyl-functionalized graphene, which modulated oxidative stress responses without causing significant harm (Yang et al. 2015). However, growth inhibition at the highest concentration (1000 mg L^{-1}) could be attributed to the accumulation of biochar particles in the gut. This could lead to energy deficits or the activation of stress pathways that limited growth. Similarly, Sanchez-Hernandez et al. (2019) reported that excessive biochar particles adversely affected enzymes in the earthworm digestive system, decreasing earthworm weight. Additionally, the insignificant changes in brood size across all treatments indicated that although DBC impacted somatic growth, it did not significantly affect reproductive output under the tested conditions. This finding is consistent with previous studies showing that some environmental stressors had a stronger impact on growth than on reproduction (Lee et al. 2024).

To further clarify the physiological mechanisms underlying DBC-induced toxicity in *C. elegans*, oxidative stress biomarkers were examined (Fig. S3). Results showed that ROS levels increased significantly and dose-dependently in the L, M, and H treatment groups, being 48.39%, 69.53%, and 93.73% higher than those in the control group (CK), respectively ($p < 0.05$). This trend indicated a pronounced oxidative stress response induced by DBC exposure. Simultaneously, the activity of antioxidant enzymes declined significantly. SOD concentrations decreased from 21.78 ± 0.31 ng mL^{-1} in CK to 18.28 ± 0.66, 15.01 ± 0.57, and 11.79 ± 0.30 ng mL^{-1} in the L, M, and H groups ($p < 0.05$), and CAT activity dropped from 813.07 ± 32.30 pg mL^{-1} in CK to 668.34 ± 34.02, 574.32 ± 18.70, and 525.66 ± 1.17 pg mL^{-1}, respectively. These results indicated that DBC exposure reduced the antioxidative capacity of nematodes while simultaneously enhancing intracellular oxidative burden.

Notably, $^1O_2$ concentrations also increased significantly with DBC exposure. Pearson correlation analysis (Fig. S4) revealed a strong positive correlation between $^1O_2$ and ROS levels ($r = 0.77$, $p < 0.01$), suggesting that singlet oxygen plays a key role in initiating ROS accumulation. Furthermore, both ROS and $^1O_2$ showed significant positive correlations with body bending frequency, whereas SOD and CAT were negatively correlated ($p < 0.05$), implying that the oxidative imbalance disrupts neuromuscular function. These physiological responses confirm oxidative stress as a central mediator of DBC-induced toxicity.

These findings align with previous studies suggesting that surface functional groups and free radical-generating potential of biochar particles could be critical determinants of biological effects (Xu et al. 2023; Jia et al. 2025). Although direct structural transformations of DBC post-ingestion were not captured in this study, the observed oxidative stress response likely stems from biochar surface reactivity rather than morphological alteration per se. The DBC is known to facilitate microbe or host–particle interactions, which can trigger the generation of reactive intermediates such as singlet oxygen ($^1O_2$) or hydroxyl radicals (–OH) (Kumari et al. 2024). These interactions provide a plausible mechanistic basis for the enhanced intracellular oxidative burden and neuromuscular disruption observed in *C.*

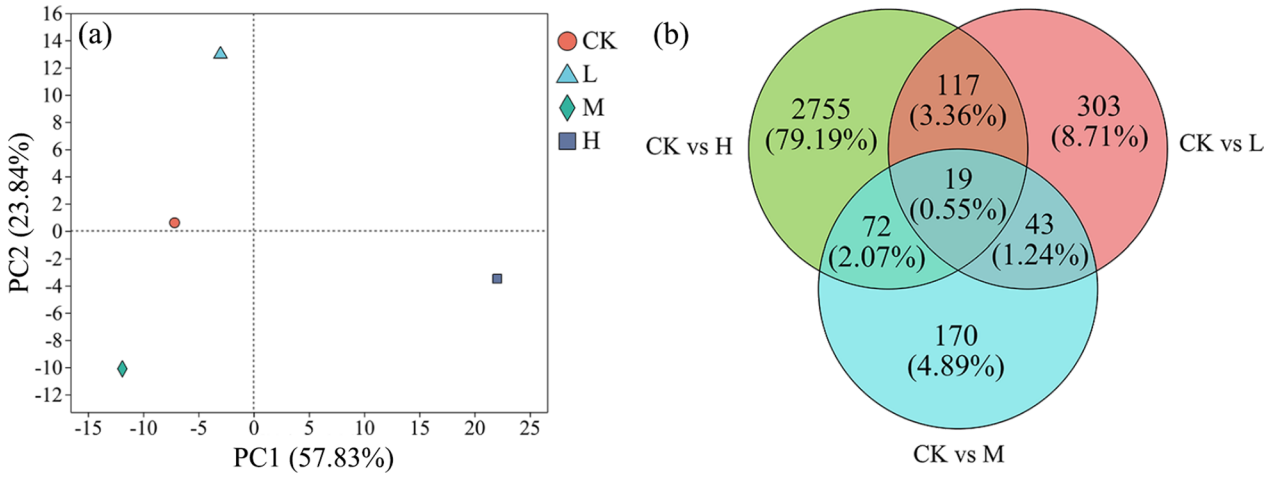

Fig. 3 Principal component analysis (**a**) and Venn diagram (**b**) for DEGs of *C. elegans* under different DBC concentrations

elegans, reinforcing the role of particle-induced redox perturbations as a key driver of DBC-mediated toxicity.

3.3 Transcriptome sequencing analysis of the effect of DBC on *C. elegans*

To explore the molecular mechanisms of the impact of DBC on nematodes, transcriptome sequencing analysis was conducted on *C. elegans* exposed to 0 (control), 250, 500 and 1000 mg L^{-1} DBC for 56 h. Differentially expressed genes (DEGs) were identified using a false discovery rate (FDR)-adjusted p value < 0.05 and an absolute fold change > 1.0 as thresholds. Compared with the control group, 482 genes (147 up- and 335 down-regulated genes), 304 genes (123 up- and 181 down-regulated genes) and 2963 genes (843 up- and 2120 down- regulated genes) were differentially expressed following the 250 mg L^{-1} (Fig. S5a), 500 mg L^{-1} (Fig. S5b) and 1000 mg L^{-1} (Fig. S5c) treatments, respectively. These results revealed a dose-dependent increase in the number of DEGs. The number of DEGs increased from 482 at 250 mg L^{-1} to 2963 at 1000 mg L^{-1}, suggesting a threshold effect wherein low or moderate concentrations of DBC weakly affected the nematode's biological systems, whereas higher concentrations induced widespread changes in gene expression.

Principal component analysis (PCA) confirmed the dose-dependent nature of the response. Significant differences were detected between the low (250 mg L^{-1}) and moderate (500 mg L^{-1}) DBC treatments when compared with the high concentration (1000 mg L^{-1}) DBC treatment (Fig. 3a). The first, second and third principal components explained 57.83%, 23.84% and 18.32% of the total variation, respectively. A Venn diagram illustrated 303 overlapping DEGs between the CK and L groups, 170 overlapping DEGs between the CK and M groups, and 2755 overlapping DEGs between the CK and H groups (Fig. 3b). This clear differentiation underscored that high DBC exposure induced more pronounced molecular changes compared to low and moderate concentrations. Moreover, the clear separation observed between the low (250 mg L^{-1}) and moderate (500 mg L^{-1}) DBC treatments from the high (1000 mg L^{-1}) DBC treatment emphasized the dose-dependent effects of DBC on nematode biology. The DEG responses were consistent with variations in body size but did not correlate with changes in reproductive capacity or body bending frequency (Fig. 2), suggesting that these physiological parameters were influenced by distinct mechanisms.

Additionally, trend analysis of the DEG data indicated that DBC affected nematode biology through various concentration-dependent mechanisms. At lower concentrations, the gene expression changes were primarily associated with metabolic processes and stress responses, whereas higher concentrations triggered a widespread activation of pathways related to cell growth and apoptosis. These findings noted that DBC influenced *C. elegans* through complex molecular pathways, including those involved in oxidative stress, immune responses, and metabolic regulation, offering a more comprehensive understanding of how DBC affect nematode biology.

3.4 Functional enrichment and pathway analysis of *C. elegans* exposed to DBC

The DEGs identified under different DBC concentrations were further annotated via GO analysis to identify functional process terms, including those in the biological process (BP), cellular component (CC), and molecular function (MF) categories. Compared to the

control group, DBC exposure resulted in the enrichment of 11 BP terms, 2 CC terms, and 7 MF terms (Fig. S6).

In the biological process (BP) category, the majority of DEGs were associated with cellular processes, metabolic processes, biological regulation, response to stimuli, and localization. These processes were directly involved in the ability of worms to respond to environmental stressors, such as DBC exposure. The alterations in these processes are consistent with findings in Mitchum et al. (2013). In particular, the upregulation of genes involved in metabolism indicated that DBC exposure increased the worms' metabolic activity, which aligned with the observed increases in body bending across all DBC concentrations, suggesting a stimulation of neuromuscular activity (Fig. S6). Furthermore, the upregulation of genes related to the response to stimuli supported the hypothesis that DBC induced a cellular stress response, potentially linked to oxidative stress (Zhao et al. 2017; Yu et al. 2022).

In the molecular function (MF) category, the enriched genes related to binding and catalytic activity indicated that DBC exposure could have altered enzymatic functions and interactions within cells. The modification of binding and catalytic activities could disrupt metabolic pathways and signal transduction, thereby potentially affecting worm growth and development (Zhu and Chin-Sang 2024). Similar observations were reported in studies examining the impact of environmental contaminants on the molecular functions of *C. elegans*, where changes in catalytic activities were linked to oxidative stress and metabolic disturbances (Yu et al. 2022). These findings were consistent with the observed phenotypic effects, such as disrupted neurodegenerative pathways at low concentrations (250 mg L^{-1}) and cell signaling disruptions at medium concentrations (500 mg L^{-1}), further linking gene expression changes to physiological responses.

Moreover, the main terms enriched in the cellular component (CC) category were related to protein-containing complexes and cellular anatomical entities. This indicated that DBC exposure may compromise the structural integrity and functionality of cellular components. This could have significant implications for the overall cellular architecture and the functionality of essential protein complexes, which were crucial for maintaining cellular homeostasis (Lettre and Hengartner 2006). This structural impact likely contributed to the observed growth inhibition at higher DBC concentrations, particularly through the induction of necrosis and cancer-related pathways at 1000 mg L^{-1} (Fig. 4).

According to further KEGG analysis, the identified DEGs were classified into the following six KEGG functional categories: organismal systems, metabolism, human diseases, genetic information processing, environmental information processing, and cellular process (Fig. S7). Compared to the CK group, the types and numbers of enriched pathways ($p < 0.01$) in the 500 mg L^{-1} and 1000 mg L^{-1} DBC treatment groups were similar and significantly greater than those in the 250 mg L^{-1} DBC treatment group. The top functional subcategories in the 500 mg L^{-1} DBC group included transport and catabolism, aging, and the endocrine system. Compared with those in the control group, the main pathways in the 1000 mg L^{-1} DBC group involved signal transduction, cell growth and death, and the immune system.

Additionally, scatter plots displayed the KEGG enrichment among different DBC groups (Fig. 4). The low concentration (250 mg L^{-1}) primarily affected oxidative phosphorylation and neurodegenerative pathways, while the medium concentration (500 mg L^{-1}) induced oxidative stress and cell signaling disruption. At the high concentration (1000 mg L^{-1}), DBC exposure led to significant enrichment in necroptosis and cancer-related pathways, indicating severe cellular damage.

In total, the DEGs identified under varying DBC concentrations were analyzed through GO and KEGG pathway analyses to explore the underlying molecular mechanisms in *C. elegans*. At lower concentrations, DBC primarily upregulated genes associated with metabolism and stress responses, correlating with increased neuromuscular activity observed in body bending assays. At higher DBC concentration, DBC exposure induced extensive changes in gene expression, including pathways related to necrosis and cancer, suggesting significant cellular damage and metabolic disruption. These findings suggested that DBC had dose-dependent effects affecting cellular integrity and metabolic regulation in *C. elegans*, providing insights into the ecological and toxicological impacts of biochar application on nematodes.

3.5 Key pathway nodes for *C. elegans* exposed to DBC

To identify critical gene modules and highly connected genes associated with body size, body bending, and brood size in *C. elegans* exposed to DBC, the Weighted Gene Co-expression Network Analysis (WGCNA) was employed based on gene expression data. Soft-threshold analysis revealed that a soft power of 12 was optimal for module detection (Fig. 5a). Following network construction and module detection, the relationships between modules and traits were also investigated (Fig. 5b, c). Out of 18 detected modules, 4 were significantly associated with body size, 2 with body

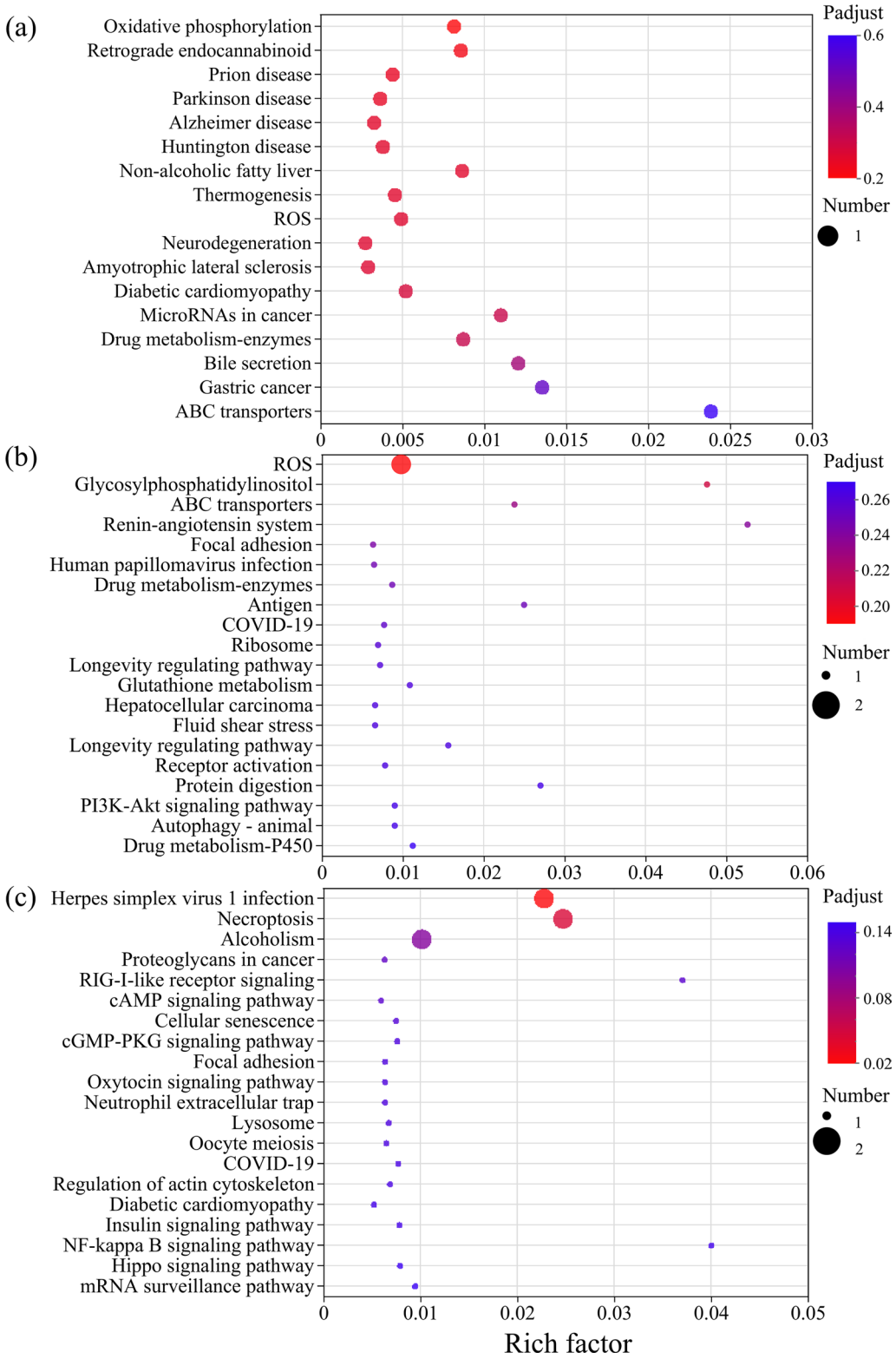

Fig. 4 KEGG pathway enrichment for the DEGs identified in *C. elegans* exposed to different DBC concentrations. **a** L: 250 mg L^{-1}; **b** M: 500 mg L^{-1}; **c** H: 1000 mg L^{-1}

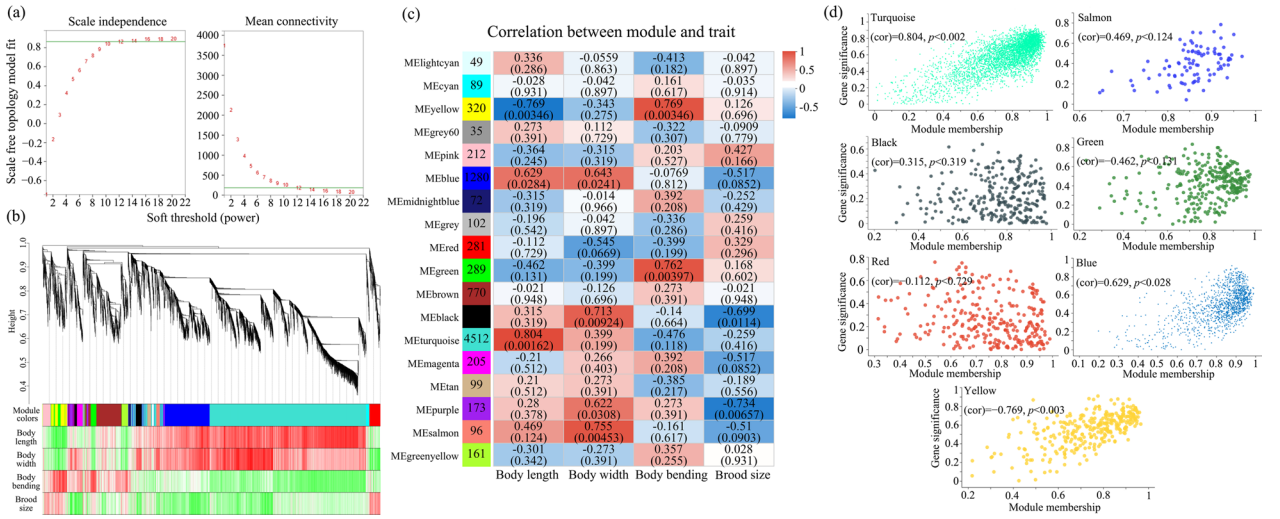

Fig. 5 Graphs produced by WGCNA. **a** Soft power detection. The graph indicates that soft powers above 12 meet the scale-free topology above 0.8. **b** Module detection and merging modules. **c** Module–trait relationship heatmap. Only those modules with strong relationships (> 0.3) were selected for further analysis. **d** Module membership versus gene significance of the highly correlated modules at specific time points

bending, and 1 with brood size. From these, we selected the top 6 modules that were highly correlated with at least one trait of *C. elegans* (Fig. 5d). Overall, the modules named "turquoise", "blue" and "yellow" were identified as significant.

DEGs identified through WGCNA were ranked based on gene significance (GS) and module significance (MS), and several genes were found to be significantly correlated with traits such as body size, body bending, and brood size (Table 2). Notably, the turquoise module, which included *dyf-11*, *dyf-13*, *dyf-19*, *ins-16*, and *atat-2*, was strongly correlated with body length. Genes from the *dyf* gene family, such as *dyf-11*, *dyf-13*, and *dyf-19*, played critical roles in intraciliary anterograde transport and cilium assembly, essential for maintaining ciliary function in *C. elegans* (Prevo et al. 2015). Specifically, proteins like DYF-11 and DYF-13 were reported to be involved in intraflagellar transport in *C. elegans,* a critical process for proper cilia function (Inglis et al. 2009). Proper ciliary function was vital for the maintenance of cell signaling, which in turn directly affected organismal growth. Disruptions in ciliary function, as caused by mutations in *dyf* genes, were often associated with developmental defects, including impaired growth and reduced body size.

Ins-16, an insulin-like peptide, was expressed in multiple developmental regions and likely played roles in systemic growth and neural development through insulin signaling, a key pathway regulating organismal growth and metabolism. Mutations in insulin-like signaling pathways have been shown to significantly affect growth rates and body size in *C. elegans* (Kimura et al. 2017). Given its expression in distal tip cells, neurons, and the pharynx, *ins-16* could have modulated developmental signaling across various tissues. Similarly, *atat-2*, encoding tubulin N-acetyltransferase, was also found to be associated with body size regulation through its impact on thigmotaxis and sensory perception (Akella et al. 2010; Akhmanova and Steinmetz 2015). The role of *atat-2* in microtubule acetylation likely helped maintain sensory neuron structure, linking neuronal integrity to overall organismal size and behavior.

In the blue module, genes *dpy-3* and *dyc-1* were strongly correlated with body length, highlighting the importance of structural components in growth regulation. *dpy-3* is a key component of the collagen trimer and always plays a crucial role in the cuticle molting cycle, directly affecting cuticle integrity and body morphology (Johnstone 2000). The cuticle, an extracellular structure essential for body shape and protection, was intricately linked to growth regulation, and any disruption in this process could lead to developmental abnormalities, including abnormal body size (Sandhu et al. 2021). In addition, *dyc-1*, a key player in muscle homeostasis and sarcomere organization, was part of the dystrophin-associated glycoprotein complex, which is crucial for muscle membrane stability during contraction (Burghes et al. 2001; Lecroisey et al. 2009). These findings suggest that both cuticle integrity and muscle integrity are essential for body length regulation. Further research would be needed to explore the interactions between these components and how they coordinate to ensure proper body length and overall health. These structural and physiological pathways are

Table 2 Top 20 significant DEGs in *C. elegans* exposed to DBC

Trait	Gene name	Module	MM	GS	Function
Body size	*dyf-13*	Turquoise	0.86	0.94	Involved in intraciliary anterograde transport and intraciliary transport in cilium assembly
	dyf-19		0.87	0.89	
	dyf-11		0.94	0.87	
	ins-16	Turquoise	0.91	0.90	Expressed in distal tip cells, the intestine, neurons, and the pharynx
	atat-2	Turquoise	0.88	0.89	Involved in thigmotaxis and expressed in ciliated neurons and touch receptor neurons
	dpy-3	Blue	0.93	0.98	Involved in cuticle development and predicted to be part of collagen trimers
	dyc-1	Blue	0.88	0.79	Involved in muscle cell cellular homeostasis; regulation of egg-laying behavior and sarcomere organization
	cat-4	Salmon	0.93	0.84	Involved in dopamine, melanin, and tetrahydrobiopterin in biosynthesis. Predicted to be active in the cytoplasm
	rnf-145	Salmon	0.91	0.82	Involved in proteasome-mediated ubiquitin-dependent protein catabolic processes
	semo-1	Black	0.86	0.77	Enables methanethiol oxidase activity and is expressed in the hypodermis
	ceh-5	Black	0.88	0.72	Involved in brain development, neuron differentiation and RNA polymerase II transcription regulation. Active in the nucleus
	tni-1	Black	0.95	0.71	Involved in backward locomotion. Part of muscle thin filament tropomyosin
Body bending	*vit-5*	Green	0.90	0.92	Predicted to enable lipid transporter activity and could be involved in lipid transport. Expressed in the intestine
	vit-6	Green	0.92	0.78	
	eral-1	Green	0.86	0.84	Involved in regulating egg-laying behavior and aerobic respiration. Located in the mitochondrial inner membrane and active in the mitochondrial matrix
	pcmd-1	Green	0.87	0.84	Expressed in the germ line
	spat-1	Green	0.84	0.78	Involved in positive regulation of the mitotic cell cycle
	vps-18	Green	0.86	0.77	Involved in endosome organization and phagosome-lysosome fusion involved in apoptotic cell clearance
	ceh-49	Yellow	0.95	0.75	Involved in RNA polymerase II transcription regulation. Active in the nucleus
	rgs-8.1	Yellow	0.93	0.73	Expressed in the PVT and intestine
	lsy-27	Yellow	0.83	0.73	Involved in neuron differentiation and DNA-templated transcription regulation. Active in the nucleus
	crn-4	Yellow	0.95	0.65	Involved in RNA catabolic process and apoptotic DNA fragmentation
	srp-1	Yellow	0.82	0.50	Enables peptidase activity and serine-type endopeptidase inhibitor activity and involved in proteolysis
Brood size	*hsp-12.6*	Red	0.84	0.82	Enables identical protein binding activity. Involved in protein refolding and heat response. Located in the cytoplasm
	ins-15	Red	0.85	0.53	Involved in signal transduction and expressed in several structures, including the egg-laying apparatus, gonad, head muscle, neurons, and the ventral nerve cord
	gcy-12	Red	0.92	0.53	Enables guanylate cyclase activity. Involved in negative regulation of dauer larval development, growth regulation, and locomotion. Expressed in excretory gland cells, ganglia, head muscle, and head neurons
	his-53	Red	0.82	0.48	Enables DNA binding activity and protein heterodimerization activity
	his-51		0.82	0.48	
	his-21		0.82	0.48	
	his-19		0.82	0.48	
	col-108	Red	0.87	0.58	Predicted to be a structural constituent of the cuticle. Predicted to be located in membranes

fundamental to understanding how physical growth is regulated in *C. elegans* and how defects in these processes may lead to developmental disorders or reduced fitness.

The strong correlations between body width and genes in the salmon and black modules, including *cat-4*, *rnf-145*, *semo-1*, *ceh-5*, and *tni-1*, suggested the existence of a multifaceted regulatory network involving neurotransmitter biosynthesis, protein degradation, and muscle function, all critical for body morphology. *cat-4*, essential for dopamine biosynthesis, impacted both neuronal and muscular physiology. Dopamine signaling was reported to affect several physiological processes, including movement and growth, likely contributing to body width regulation (Sanyal et al. 2004; Baker et al. 2012). Furthermore, *rnf-145*, a ubiquitin ligase, regulates protein degradation and is expressed in muscle and

nervous system tissues, indicating its role in maintaining protein homeostasis and facilitating growth regulation (Zhang et al. 2020). Disruption of this pathway could lead to abnormal protein turnover, affecting muscle function and consequently body size and morphology. *semo-1*, localized in the hypodermis, and *ceh-5*, a transcription factor regulating neuronal differentiation, contributed to tissue development, further linking growth regulation to cell differentiation and tissue organization (Aquino-Nunez et al. 2020; Philipp et al. 2022). Additionally, *tni-1*, associated with contraction via troponin–tropomyosin interactions, was essential for locomotion and linked muscular function directly to body structure (Matsunaga et al. 2016). Together, these genes formed an intricate network that coordinated multiple aspects of growth and body width regulation, encompassing neurotransmitter biosynthesis, protein degradation, and muscle function. These findings suggested the interdependence of molecular and physiological pathways that regulate body morphology in *C. elegans*.

WGCNA further revealed that genes in the green and yellow modules were strongly correlated with the frequency of body bending in *C. elegans*, which was a key indicator of worm health and muscle function. In the green module, *vit-5* and *vit-6*, both involved in lipid transport, were likely related to muscle regulation through the modulation of lipid metabolism. Lipids are essential for maintaining membrane integrity and energy homeostasis, which are crucial for muscle contraction. *eral-1*, which is essential for rRNA binding and mitochondrial function, regulates energy metabolism, a process directly linked to muscle contraction and movement (Chatzispyrou et al. 2017). Furthermore, the involvement of *pat-1* in cell cycle regulation suggested that developmental processes could also impact muscle function, linking cell proliferation and differentiation to muscle physiology. In the yellow module, *ceh-49* and *lsy-27*, both encoding transcription factors, regulated neuronal differentiation and transcription, affecting muscle contraction (Ramakrishnan and Okkema 2014). The influence of these transcription factors on neuronal signaling and muscle activity indicated that a neuromuscular interplay was critical for maintaining body movement and health. Additionally, the role of *rgs-8.1* in neurotransmission supported the integration of signals with muscle function. The roles of *crn-4* and *srp-1*, which were involved in RNA degradation and protein turnover, emphasized the importance of molecular regulation in maintaining muscle integrity and function (Pak et al. 2004; Huang et al. 2016). These findings suggested that lipid metabolism, transcription regulation, and protein turnover were pivotal for maintaining muscle health and body movement.

Brood size, a key indicator of reproductive success, was significantly correlated with the red module, particularly genes such as *hsp-12.6*, *ins-15*, *gcy-12*, and *col-108*. *hsp-12.6*, a protein chaperone, played a crucial role in protein refolding under stress conditions, and its expression in reproductive tissues suggested a direct influence on fertility and offspring count (Murphy et al. 2003). Heat shock proteins, including Hsp-12.6, were involved in the stress response, helping cells cope with environmental challenges and thereby ensuring reproductive success under fluctuating conditions. Similarly, *ins-15,* expressed in the gonads and egg-laying apparatus, likely affected reproductive output through hormonal regulation (Pierce et al. 2001). *gcy-12,* involved in guanylate cyclase activity, regulated dauer formation and growth, which in turn affected developmental decisions and reproductive success (Yu et al. 1997; Fujiwara et al. 2010). Moreover, *col-108*, which was involved in environmental adaptation, played a crucial role in maintaining organismal integrity and ensuring reproductive success (Johnstone 2000). Furthermore, *his* family genes (*his-53*, *his-51*, *his-21*, and *his-19*) were involved in chromatin organization and DNA binding, with their roles in regulating gene expression likely impacted fertility and progeny numbers by influencing the development and function of reproductive tissue (Chu et al. 2006). Collectively, these findings implied that the intricate balance between stress responses, hormonal regulation, and developmental pathways drove reproductive success in *C. elegans*.

This study integrated WGCNA with DEG analyses to identify key genetic modules and their associated traits in *C. elegans.* WGCNA identified gene modules that were highly correlated with specific traits, such as body width, bending frequency, and brood size, allowing for a systems-level view of the genetic networks involved. For example, the identification of *cat-4*, *rnf-145*, and *tni-1* in the regulation of body size suggested the importance of neurotransmitter biosynthesis, protein degradation, and muscle function in growth regulation, as noted by WGCNA. These findings were further elucidated through DEG analysis, which identified key regulatory molecules, such as dopamine and ubiquitin ligases, involved in muscle function and body morphology. Similarly, the roles of lipid metabolism, transcription regulation, and protein turnover in muscle function and health were reinforced through both WGCNA and DEG analyses, providing a comprehensive view of the biological pathways involved. In the context of reproductive success, the identification of genes such as *hsp-12.6*, *ins-15*, and *gcy-12* further emphasized the complex interplay among stress response pathways, hormonal regulation, and growth regulation. Thus, by combining the two analytical methods, the study

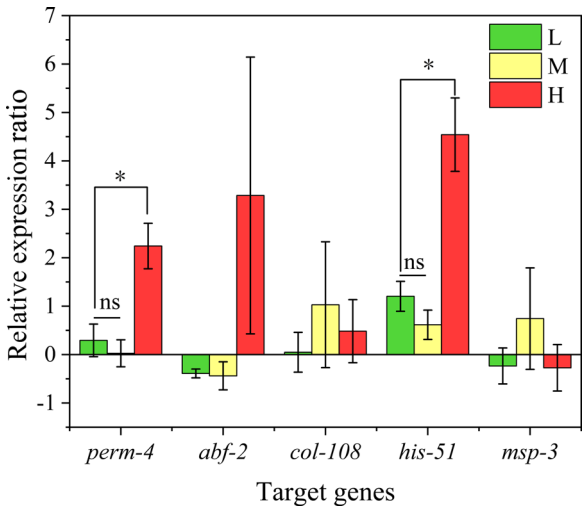

Fig. 6 Different gene expression patterns of *C. elegans* exposed to different treatments were determined via qPCR

revealed how genetic and environmental factors interact to influence the development, behavior, and reproductive success of *C. elegans*.

3.6 Analysis of target genes related to DBC-exposed *C. elegans*

To validate the transcriptome sequencing results and further investigate the molecular mechanisms of DBC on *C. elegans*, real-time quantitative PCR (qRT–PCR) was performed on five genes: *perm-4*, *abf-2*, *col-108*, *his-51*, and *msp-3* (Fig. 6). These genes were involved in various biological processes, including reproduction, immune response, cuticle structure, chromatin remodeling, and sperm motility.

Among the identified genes, *perm-4* was an egg yolk-related gene that was significantly upregulated under treatment with 1000 mg L^{-1} DBC. This upregulation suggested that DBC might have enhanced yolk protein synthesis, which is vital for nutrient storage and embryo development. The increased expression of *perm-4* indicated a stress-induced or metabolic adaptation aimed at maintaining reproductive capacity under adverse conditions.

The *abf-2* gene, known for its role in the immune response, is primarily expressed in the pharynx and excretory cells (Tomisawa et al. 2013). In response to low and medium concentrations of DBC, *abf-2* expression was lower than that in the control, but significant differences were observed under high concentration DBC. This concentration-dependent variation indicated a potential immunomodulatory effect of DBC. At lower concentrations, the reduced expression of *abf-2* may reflect a compensatory or adaptive mechanism to maintain immune homeostasis. In contrast, the upregulation at high concentrations likely represented an activation of immune responses to counteract the heightened stress induced by excessive DBC exposure.

The *col-108* gene is part of a collagen triplet and mainly affects the structure of the cuticle. In this study, *col-108* expression did not show significant changes upon DBC exposure. The lack of significant impact may be due to the small particle size of the biochar micronanoparticles, which may not be sufficient to cause direct mechanical disruption of the cuticle. However, it is important to consider that subcellular or molecular interactions could still have indirectly affected cuticle integrity without altering *col-108* expression levels. Similarly, *msp-3*, which is associated with sperm mobility and reproduction, also exhibited alterations in expression, although its specific changes in response to biochar exposure were less pronounced compared to those of other target genes.

Furthermore, the *his-51* gene encodes a histone protein critical for DNA binding and chromatin structure within the nucleosome. Significant alterations in *his-51* expression were observed only at the highest DBC concentration (1000 mg L^{-1}), indicating that DBC exposure may influence chromatin remodeling and DNA-related processes. This suggested potential epigenetic effects, where biochar-induced transcriptional reprogramming modified chromatin dynamics, leading to changes in gene regulation. Disruption of histone function could alter gene expression profiles, underpinning broader physiological effects such as modified stress responses and developmental processes.

Overall, qRT-PCR validation of target genes revealed that DBC, particularly at relatively high concentrations, could modulate key genetic pathways in *C. elegans*, impacting reproductive processes, immune responses, chromatin remodeling, and sperm motility. This study suggested molecular mechanisms through which DBC affected organismal physiology. These findings provided a molecular framework for understanding how biochar exposure influenced *C. elegans* at the gene expression level. Future research could explore the interactions between dissolved biochar and these genetic pathways in more detail, including the role of environmental stressors in shaping gene expression and the potential for DBC to induce epigenetic changes.

4 Conclusion

This study provides novel insights into the dose-dependent effects of dissolved biochar (DBC) on *C. elegans,* revealing both its potential benefits and risks. At lower concentrations (< 500 mg L^{-1}), DBC promoted the nematode growth and locomotor activity, likely due to the additional nutrient availability or triggering mild physiological stimulation. However, at higher concentrations, DBC posed significant risks by disrupting nematode metabolism processes, and inducing widespread transcriptional variations. Furthermore, transcriptomic analysis identified key differentially expressed genes (DEGs) involved in cellular metabolism, biological regulation, and catalytic activity, reinforcing the dual effects of DBC. These findings highlight the necessity of careful biochar application in agriculture to maximize its benefits while minimizing potential ecological risks. Future research should further explore the long-term ecological impact of DBC, particularly on soil nematode communities and other non-target organisms, to better understand its broader implications in soil health and ecosystem resilience.

Supplementary Information

The online version contains supplementary material available at https://doi.org/10.1007/s42773-025-00493-9.

Additional file 1.

Additional file 2.

Acknowledgements
The authors extend their appreciation to the Chinese Academy of Agricultural Sciences Innovation Program (Agro-Environmental Protection Institute).

Author contributions
All the authors contributed to the conception and design of the study, material preparation, data collection, and analysis. Wang Xinrui wrote the first draft of the manuscript. All the authors commented on previous versions, and Jie Li made the final version. All the authors read and approved the final manuscript.

Funding
This study was funded by (1) National Science Foundation of China [42207048]; (2) The Agricultural Science and Technology Innovation Program (ASTIP) [CAAS-202408-04].

Data availability
Data are added as supplementary material.

Declarations

Competing interests
The authors have no relevant financial or non-financial interests to disclose.

Author details
[1]Agro-Environmental Protection Institute, Ministry of Agriculture and Rural Affairs, Tianjin 300191, China. [2]College of Life Sciences, Nankai University, Tianjin 30071, China.

Received: 9 October 2024 Revised: 19 June 2025 Accepted: 25 June 2025
Published online: 26 August 2025

References

Akella JS, Wloga D, Kim J, Starostina NG, Lyons-Abbott S, Morrissette NS, Dougan ST, Kipreos ET, Gaertig J (2010) MEC-17 is an α-tubulin acetyltransferase. Nature 467:218-U111. https://doi.org/10.1038/nature09324

Akhmanova A, Steinmetz MO (2015) Control of microtubule organization and dynamics: two ends in the limelight. Nat Rev Mol Cell Biol 16:711–726. https://doi.org/10.1038/nrm4084

Alharbi HA, Alotaibi KD, El-Saeid MH, Giesy JP (2023) Polycyclic Aromatic Hydrocarbons (PAHs) and metals in diverse biochar products: effect of feedstock type and pyrolysis temperature. Toxics 11:14. https://doi.org/10.3390/toxics11020096

Aquino-Nunez W, Mielko ZE, Dunn T, Santorella EM, Hosea C, Leitner L, McCalla D, Simms C, Verola WM, Vijaykumar S, et al. (2020) cnd-1/NeuroD1 Functions with the Homeobox Gene ceh-5/Vax2 and Hox Gene *ceh-13*/labial To Specify Aspects of RME and DD Neuron Fate in *Caenorhabditis elegans*. G3 Genes Genomes Genet 10: 3071–3085. https://doi.org/10.1534/g3.120.401515

Baker RH, Britton C, Roberts B, Loer CM, Matthews JB, Nisbet AJ (2012) Melanisation of *Teladorsagia circumcincta* larvae exposed to sunlight: a role for GTP-cyclohydrolase in nematode survival. Int J Parasit 42:887–891. https://doi.org/10.1016/j.ijpara.2012.06.005

Burghes AHM, Vaessin HEF, de la Chapelle A (2001) Genetics—the land between Mendelian and multifactorial inheritance. Science 293:2213–2214. https://doi.org/10.1126/science.1065930

Chatzispyrou IA, Alders M, Guerrero-Castillo S, Perez RZ, Haagmans MA, Mouchiroud L, Koster J, Ofman R, Baas F, Waterham HR et al (2017) A homozygous missense mutation in *ERAL1*, encoding a mitochondrial rRNA chaperone, causes Perrault syndrome. Hum Mol Genet 26:2541–2550. https://doi.org/10.1093/hmg/ddx152

Chu DS, Liu HB, Nix P, Wu TF, Ralston EJ, Yates JR, Meyer BJ (2006) Sperm chromatin proteomics identifies evolutionarily conserved fertility factors. Nature 443:101–105. https://doi.org/10.1038/nature05050

Da Costa VB, Ogura AP, Alexandre DS, Soares MB, Alleoni LRF, Espíndola ELG, Pinto TJD (2024) How much biochar is safe? Exploring potential ecotoxicological consequences for soil invertebrates and plants. Appl Soil Ecol 202:9. https://doi.org/10.1016/j.apsoil.2024.105552

Dong MY, Jiang MY, He LZ, Zhang ZR, Gustave W, Vithanage M, Niazi NK, Chen B, Zhang XK, Wang HL et al (2025) Challenges in safe environmental applications of biochar: identifying risks and unintended consequence. Biochar 7:20. https://doi.org/10.1007/s42773-024-00412-4

Ellegaard-Jensen L, Jensen KA, Johansen A (2012) Nano-silver induces dose-response effects on the nematode *Caenorhabditis elegans*. Ecotox Environ Safe 80:216–223. https://doi.org/10.1016/j.ecoenv.2012.03.003

Fujiwara M, Teramoto T, Ishihara T, Ohshima Y, McIntire SL (2010) A novel zf-MYND protein, CHB-3, mediates guanylyl cyclase localization to sensory cilia and controls body size of *Caenorhabditis elegans*. PLoS Genet 6:e1001211. https://doi.org/10.1371/journal.pgen.1001211

Gu Y, Jiang Y, Chen X, Li L, Chen H, Chen J, Wang C, Yu J, Chen C, Li H (2024) Generation of environmentally persistent free radicals on photoaged tire wear particles and their neurotoxic effects on neurotransmission in *Caenorhabditis elegans*. Environ Int 186:108640. https://doi.org/10.1016/j.envint.2024.108640

Guggenberger G, Rodionov A, Shibistova O, Grabe M, Kasansky OA, Fuchs H, Mikheyeva N, Zrazhevskaya G, Flessa H (2008) Storage and mobility of black carbon in permafrost soils of the forest tundra ecotone in Northern Siberia. Glob Change Biol 14:1367–1381. https://doi.org/10.1111/j.1365-2486.2008.01568.x

Hemmatzadeh M, Mohammadiazarm H, Ghasemi SA, Rezaie A (2024) Influence of humic acids on growth performance, bravery, stress resistance, antioxidant activity, and immune gene expression in male Siamese fighting fish (Betta splendens). Aquacult Rep. https://doi.org/10.1016/j.aqrep.2024.102286

Hou S, Wang J, Dai J, Boussafir M, Zhang C (2022) Combined effects of earthworms and biochar on PAHs-contaminated soil remediation: a review. Soil Ecol Lett. https://doi.org/10.1007/s42832-022-0158-y

Huang KW, Hsu KC, Chu LY, Yang JM, Yuan HS, Hsiao YY (2016) Identification of Inhibitors for the DEDDh Family of Exonucleases and a Unique Inhibition Mechanism by Crystal Structure Analysis of CRN-4 Bound with 2-Morpholin-4-ylethanesulfonate (MES). J Med Chem 59:8019–8029. https://doi.org/10.1021/acs.jmedchem.6b00794

Inglis PN, Blacque OE, and Leroux MR (2009). Functional Genomics of Intraflagellar Transport-Associated Proteins in *C. elegans*. In: King SM, Pazour GJ (eds.) Cilia: Model Organisms and Intraflagellar Transport, (San Diego: Elsevier Academic Press Inc), pp 267–304

Jeffery S, van de Voorde TFJ, Harris WE, Mommer L, Van Groenigen JW, De Deyn GB, Ekelund F, Briones MJI, Bezemer TM (2022) Biochar application differentially affects soil micro-, meso-macro-fauna and plant productivity within a nature restoration grassland. Soil Biol Biochem. https://doi.org/10.1016/j.soilbio.2022.108789

Jia X, Zhang B, Han Y, Guan J, Gao H, Guo P (2025) Role of reactive oxygen species (ROS) on biochar enhanced chromium phytoremediation in the soil-plant system: exploration on detoxification mechanism. Environ Int 199:109471

Jiang SF, Hao HC, Chen S, Chen YL, Jiang H (2024) Mechanistic elucidation and tuning pathway of environmentally persistent free radicals during sewage sludge pyrolysis. J Anal Appl Pyrolysis 179:10. https://doi.org/10.1016/j.jaap.2024.106502

Johnstone IL (2000) Cuticle collagen genes-: expression in *Caenorhabditis elegans*. Trends Genet 16:21–27. https://doi.org/10.1016/s0168-9525(99)01857-0

Kim D, Landmead B, Salzberg SL (2015) HISAT: A fast spliced aligner with low memory requirements. Nat Methods 12:357–U121. https://doi.org/10.1038/NMETH.3317

Kimura K, Mamane A, Sasaki T, Sato K, Takagi J, Niwayama R, Hufnagel L, Shimamoto Y, Joanny JF, Uchida S et al (2017) Endoplasmic-reticulum-mediated microtubule alignment governs cytoplasmic streaming. Nat Cell Biol 19:399–406. https://doi.org/10.1038/ncb3490

Kumari T, Phogat D, Phogat J, Shukla V (2024) Biochar & fly ash amendments lower mortality and increase antioxidant activity in chlorpyrifos-exposed earthworms. Appl Biol Chem 67:65. https://doi.org/10.1186/s13765-024-00909-3

Lecroisey C, Mariol MC, Schwab Y, Labouesse M, Ségalat L, Gieseler K (2009) DYC-1 and ZYX-1, new actors of muscle degeneration in *Caenorhabditis elegans*. Neuromusc Disord 19:639–639. https://doi.org/10.1016/j.nmd.2009.06.296

Lee I, Knickerbocker AC, Depew CR, Martin EL, Dicent J, Miller GW, Bucher ML (2024) Effect of altered production and storage of dopamine on development and behavior in *C. elegans*. Front Toxicol 6:17. https://doi.org/10.3389/ftox.2024.1374866

Lehmann J (2007) Bio-energy in the black. Front Ecol Environ 5:381–387. https://doi.org/10.1890/1540-9295(2007)5[381:Bitb]2.0.Co;2

Lehmann J, Rillig MC, Thies J, Masiello CA, Hockaday WC, Crowley D (2011) Biochar effects on soil biota—a review. Soil Biol Biochem 43:1812–1836. https://doi.org/10.1016/j.soilbio.2011.04.022

Lettre G, Hengartner MO (2006) Developmental apoptosis in *C. elegans*: a complex CEDnario. Nat Rev Mol Cell Biol 7:97–108. https://doi.org/10.1038/nrm1836

Li J, Chen YX, Zhang GL, Ruan WB, Shan SJ, Lai X, Yang DL, Yu ZG (2020) Integration of behavioural tests and transcriptome sequencing of *C. elegans* reveals how the nematode responds to peanut shell biochar amendment. Sci Total Environ 707:11. https://doi.org/10.1016/j.scitotenv.2019.136024

Li B, Dewey CN (2011) RSEM: Accurate Transcript Quantification from RNA-Seq Data with or without a Reference Genome. BMC Bioinform 12:323. https://doi.org/10.1186/1471-2105-12-323

Li HJ, Li H, Zuo N, Lang D, Du W, Zhang P, Pan B (2024a) Can the concentration of environmentally persistent free radicals describe its toxicity to *Caenorhabditis elegans*? Evidence provided by neurotoxicity and oxidative stress. J Hazard Mater 469:9. https://doi.org/10.1016/j.jhazmat.2024.133823

Li H, Liu Y, TaoYuan LY, Li T, Yan J, Yang C (2024b) Insights into the characteristics and toxicity of microalgal biochar-derived dissolved organic matter by spectroscopy and machine learning. Sci Total Environ 957:177648. https://doi.org/10.1016/j.scitotenv.2024.177648

Li L, Ma R, Yuan Y, Yao Q, Han Y, Cao H, Qi J (2024c) Neurotoxicity induced by aged microplastics from plastic bowls: abnormal neurotransmission in *Caenorhabditis elegans*. Sci Total Environ 952:175939. https://doi.org/10.1016/j.scitotenv.2024.175939

Lian F, Xing BS (2017) Black Carbon (Biochar) in water/soil environments: molecular structure, sorption, stability, and potential risk. Environ Sci Technol 51:13517–13532. https://doi.org/10.1021/acs.est.7b02528

Lian F, Xing BS (2024) From Bulk to Nano: formation, Features, and Functions of Nano-Black Carbon in Biogeochemical Processes. Environ Sci Technol 58:15910–15925. https://doi.org/10.1021/acs.est.4c07027

Lian F, Yu WC, Wang ZY, Xing BS (2019) New insights into black carbon nanoparticle-induced dispersibility of goethite colloids and configuration-dependent sorption for phenanthrene. Environ Sci Technol 53:661–670. https://doi.org/10.1021/acs.est.8b05066

Lieke T, Zhang XC, Steinberg CEW, Pan B (2018) Overlooked Risks of Biochars: persistent Free Radicals trigger Neurotoxicity in *Caenorhabditis elegans*. Environ Sci Technol 52:7981–7987. https://doi.org/10.1021/acs.est.8b01338

Liu H, Du X, Li Y, Han X, Li B, Zhang X, Li Q, Liang W (2022a) Organic substitutions improve soil quality and maize yield through increasing soil microbial diversity. J Clean Prod. https://doi.org/10.1016/j.jclepro.2022.131323

Liu X, Ge P, Lu Z, Yang R, Liu Z, Zhao F, Chen M (2022b) Reproductive toxicity and underlying mechanisms of fine particulate matter (PM(2.5)) on Caenorhabditis elegans in different seasons. Ecotoxicol Environ Saf 248:114281. https://doi.org/10.1016/j.ecoenv.2022.114281

Liu H, Wang Y, Wang SX, Wu J, Wang YL (2024a) Release characteristics of biochar-derived dissolved organic matter and its impact on Cr adsorption and reduction. RSC Adv 14:38171–38182. https://doi.org/10.1039/d4ra06172a

Liu MY, Liu XC, Hu YL, Zhang Q, Farooq U, Qi ZC, Lu LT (2024b) Mobility of biochar-derived dissolved organic matter and its effects on sulfamerazine transport through saturated soil porous media. Environ Sci Process Impacts 26:2264–2278. https://doi.org/10.1039/d4em00143e

Long XX, Yu ZN, Liu SW, Gao T, Qiu RL (2024) A systematic review of biochar aging and the potential eco-environmental risk in heavy metal contaminated soil. J Hazard Mater 472:134345. https://doi.org/10.1016/j.jhazmat.2024.134345

Love MI, Huber W, Anders S (2014) Moderated estimation of fold change and dispersion for RNA-seq data with DESeq2. Genome Biol 15:550. https://doi.org/10.1186/s13059-014-0550-8

Ma SQ, Jing FQ, Sohi SP, Chen JW (2019) New insights into contrasting mechanisms for PAE adsorption on millimeter, micron- and nano-scale biochar. Environ Sci Pollut Res 26:18636–18650. https://doi.org/10.1007/s11356-019-05181-3

Mani R, Ezhumalai D, Muthusamy G, Namasivayam E (2024) Neuroprotective effect of biogenically synthesized ZnO nanoparticles against oxidative stress and β-amyloid toxicity in transgenic Caenorhabditis elegans. Biotechnol Appl Biochem 71:132–146. https://doi.org/10.1002/bab.2527

Matsunaga Y, Honda Y, Honda S, Iwasaki T, Qadota H, Benian GM, Kawano T (2016) Diapause is associated with a change in the polarity of secretion of insulin-like peptides. Nat Commun 7:8. https://doi.org/10.1038/ncomms10573

Mitchum MG, Hussey RS, Baum TJ, Wang XH, Elling AA, Wubben M, Davis EL (2013) Nematode effector proteins: an emerging paradigm of parasitism. New Phytol 199:879–894. https://doi.org/10.1111/nph.12323

Murphy CT, McCarroll SA, Bargmann CI, Fraser A, Kamath RS, Ahringer J, Li H, Kenyon C (2003) Genes that act downstream of DAF-16 to influence the lifespan of *Caenorhabditis elegans*. Nature 424:277–284. https://doi.org/10.1038/nature01789

Nawa M, Matsuoka M (2012) The method of the body bending assay using caenorhabditis elegans. Bio Protocol 2:e253. https://doi.org/10.21769/BioProtoc.253

Nepal J, Ahmad W, Munsif F, Khan A, Zou ZY (2023) Advances and prospects of biochar in improving soil fertility, biochemical quality, and environmental applications. Front Environ Sci 11:17. https://doi.org/10.3389/fenvs.2023.1114752

Ng LYF, Ariffin H, Yasim-Anuar TAT, Farid MAA, Hassan MA (2022) High-Energy Ball Milling for High Productivity of Nanobiochar from Oil Palm Biomass. Nanomaterials 12:11. https://doi.org/10.3390/nano12183251

Pak SC, Kumar V, Tsu C, Luke CJ, Askew YS, Askew DJ, Mills DR, Bromme D, Silverman GA (2004) SRP-2 is a cross-class inhibitor that participates in

postembryonic development of the nematode Caenorhabditis elegans: initial characterization of the clade L serpins. J Biol Chem 279:15448–15459. https://doi.org/10.1074/jbc.M400261200
Perni M, van der Goot A, Limbocker R, van Ham TJ, Aprile FA, Xu CK, Flagmeier P, Thijssen K, Sormanni P, Fusco G et al (2021) Comparative Studies in the A30P and A53T α-Synuclein *C. elegans* Strains to Investigate the Molecular Origins of Parkinson's Disease. Front Cell Dev Biol 9:10. https://doi.org/10.3389/fcell.2021.552549
Philipp TM, Gong W, Kohnlein K, Ohse VA, Muller FI, Priebs J, Steinbrenner H, Klotz LO (2022) SEMO-1, a novel methanethiol oxidase in *Caenorhabditis elegans*, is a pro-aging factor conferring selective stress resistance. BioFactors 48:699–706. https://doi.org/10.1002/biof.1836
Pierce SB, Costa M, Wisotzkey R, Devadhar S, Homburger SA, Buchman AR, Ferguson KC, Heller J, Platt DM, Pasquinelli AA et al (2001) Regulation of DAF-2 receptor signaling by human insulin and *ins-1*, a member of the unusually large and diverse *C. elegans* insulin gene family. Genes Dev 15:672–686. https://doi.org/10.1101/gad.867301
Prevo B, Mangeol P, Oswald F, Scholey JM, Peterman EJG (2015) Functional differentiation of cooperating kinesin-2 motors orchestrates cargo import and transport in *C. elegans* cilia. Nat Cell Biol 17:1536–1545. https://doi.org/10.1038/ncb3263
Prodana M, Silva C, Gravato C, Verheijen FGA, Keizer JJ, Soares A, Loureiro S, Bastos AC (2019) Influence of biochar particle size on biota responses. Ecotox Environ Safe 174:120–128. https://doi.org/10.1016/j.ecoenv.2019.02.044
Qin YX, Li GY, An TC, Yang ZF (2021) Advances in ecological and health risks of biochar during environmental applications. Chin Sci Bull-Chin 66:5–20. https://doi.org/10.1360/tb-2020-0617
Ramakrishnan K, Okkema PG (2014) Regulation of *C. elegans* Neuronal Differentiation by the ZEB-Family Factor ZAG-1 and the NK-2 Homeodomain Factor CEH-28. PLoS ONE 9:17. https://doi.org/10.1371/journal.pone.0113893
Rombolà AG, Greggio N, Fabbri D, Facchin A, Torri C, Pulcher R, Carlini C, Balugani E, Marazza D, Zannoni D et al (2023) Changes of labile, stable and water-soluble fractions of biochar after two years in a vineyard soil. Environ Sci-Adv 2:1587–1599. https://doi.org/10.1039/d3va00197k
Sanchez-Hernandez JC, Cares XA, Pérez MA, del Pino JN (2019) Biochar increases pesticide-detoxifying carboxylesterases along earthworm burrows. Sci Total Environ 667:761–768. https://doi.org/10.1016/j.scitotenv.2019.02.402
Sandhu A, Badal D, Sheokand R, Tyagi S, Singh V (2021) Specific collagens maintain the cuticle permeability barrier in *Caenorhabditis elegans*. Genetics. https://doi.org/10.1093/genetics/iyaa047
Sanyal S, Wintle RF, Kindt KS, Nuttley WM, Arvan R, Fitzmaurice P, Bigras E, Merz DC, Hébert TE, van der Kooy D et al (2004) Dopamine modulates the plasticity of mechanosensory responses in *Caenorhabditis elegans*. Embo J 23:473–482. https://doi.org/10.1038/sj.emboj.7600057
Singh RP, Ahsan M, Mishra D, Pandey V, Anupama YA, Khare P (2022) Ameliorative effects of biochar on persistency, dissipation, and toxicity of atrazine in three contrasting soils. J Environ Manage 303:11. https://doi.org/10.1016/j.jenvman.2021.114146
Tian YX, Guo X, Ma J, Liu QY, Li SJ, Wu YH, Zhao WH, Ma SY, Chen HY, Guo F (2022) Characterization of biochar-derived organic matter extracted with solvents of differing polarity via ultrahigh-resolution mass spectrometry. Chemosphere 307:135785. https://doi.org/10.1016/j.chemosphere.2022.135785
Tomisawa S, Hojo E, Umetsu Y, Ohki S, Kato Y, Miyazawa M, Mizuguchi M, Kamiya M, Kumaki Y, Kikukawa T (2013) Overexpression of an antimicrobial peptide derived from *C. elegans* using an aggregation-prone protein coexpression system. AMB Express 3:8. https://doi.org/10.1186/2191-0855-3-45
Wang ZW, Li J, Zhang GL, Zhi YC, Yang DL, Lai X, Ren TZ (2020) Characterization of Acid-Aged Biochar and Its Ammonium Adsorption in an Aqueous Solution. Materials 13:17. https://doi.org/10.3390/ma13102270
Woodruff GC, Willis JH, Phillips PC (2018) Dramatic evolution of body length due to postembryonic changes in cell size in a newly discovered close relative of *Caenorhabditis elegans*. Evol Lett 2:427–441. https://doi.org/10.1002/evl3.67
Xu YL, Lu XF, Su GJ, Chen X, Meng J, Li QQ, Wang CX, Shi B (2023) Scientific and regulatory challenges of environmentally persistent free radicals: from formation theory to risk prevention strategies. J Hazard Mater. https://doi.org/10.1016/j.jhazmat.2023.131674
Yang JN, Zhao YL, Wang YW, Wang HF, Wang DY (2015) Toxicity evaluation and translocation of carboxyl functionalized graphene in *Caenorhabditis elegans*. Toxicol Res 4:1498–1510. https://doi.org/10.1039/c5tx00137d
Yang F, Wang CP, Sun HW (2021) A comprehensive review of biochar-derived dissolved matters in biochar application: production, characteristics, and potential environmental effects and mechanisms. J Environ Chem Eng 9:10. https://doi.org/10.1016/j.jece.2021.105258
Yu S, Avery L, Baude E, Garbers DL (1997) Guanylyl cyclase expression in specific sensory neurons: a new family of chemosensory receptors. Proc Natl Acad Sci USA 94:3384–3387. https://doi.org/10.1073/pnas.94.7.3384
Yu YJ, Chen HB, Hua X, Dang Y, Han YJ, Yu ZL, Chen XC, Ding P, Li H (2020) Polystyrene microplastics (PS-MPs) toxicity induced oxidative stress and intestinal injury in nematode *Caenorhabditis elegans*. Sci Total Environ 726:8. https://doi.org/10.1016/j.scitotenv.2020.138679
Yu Y, Chen H, Hua X, Wang C, Dong C, Xie D, Tan S, Xiang M, Li H (2022) A review of the reproductive toxicity of environmental contaminants in *Caenorhabditis elegans*. Hyg Environ Health Adv. https://doi.org/10.1016/j.heha.2022.100007
Zhang G, Zhang Q, Sun K, Liu X, Zheng W, Zhao Y (2011) Sorption of simazine to corn straw biochars prepared at different pyrolytic temperatures. Environ Pollut 159:2594–2601. https://doi.org/10.1016/j.envpol.2011.06.012
Zhang FS, Li YX, Zhang GX, Li W, Yang LS (2017) The importance of nano-porosity in the stalk-derived biochar to the sorption of 17β-estradiol and retention of it in the greenhouse soil. Environ Sci Pollut Res 24:9575–9584. https://doi.org/10.1007/s11356-017-8630-4
Zhang A, Guan Z, Ockerman K, Dong P, Guo J, Wang Z, Yan D (2020) Regulation of glial size by eicosapentaenoic acid through a novel Golgi apparatus mechanism. PLoS Biol 18:e3001051. https://doi.org/10.1371/journal.pbio.3001051
Zhang Y, Zhao C, Zhang H, Lu Q, Zhou JJ, Liu R, Wang SZ, Pu YP, Yin LH (2021) Trans-generational effects of copper on nerve damage in *Caenorhabditis elegans*. Chemosphere 284:13. https://doi.org/10.1016/j.chemosphere.2021.131324
Zhang R, Zhang R, Zimmerman AR, Wang H, Gao B (2023) Applications, impacts, and management of biochar persistent free radicals: a review. Environ Pollut 327:121543. https://doi.org/10.1016/j.envpol.2023.121543
Zhao L, Rui Q, Wang DY (2017) Molecular basis for oxidative stress induced by simulated microgravity in nematode *Caenorhabditis elegans*. Sci Total Environ 607:1381–1390. https://doi.org/10.1016/j.scitotenv.2017.07.088
Zhu R, Chin-Sang ID (2024) *C.elegans* insulin-like peptides. Mol Cell Endocrinol 585:11. https://doi.org/10.1016/j.mce.2024.112173